Lattice Monte Carlo Simulations of the Gyroid Phase in Monodisperse and Bidisperse Block Copolymer Systems

Francisco J. Martínez-Veracoechea and Fernando A. Escobedo*

School of Chemical and Biomolecular Engineering, Cornell University, Ithaca, New York 14853

Received June 9, 2005; Revised Manuscript Received July 29, 2005

ABSTRACT: Lattice Monte Carlo (MC) simulations in the NVT ensemble together with a coarse-grained model of the block copolymer chains are used to explore the phase diagram of pure and bidisperse diblock copolymer melts as a function of temperature and block volume fraction. In the pure systems, we found that the gyroid phase is stable in only a narrow region of the phase diagram. Through the analysis of the structure of the channels and nodes formed by the minority component in the gyroid phase, we found evidence of "packing frustration" of the chains inside each such node, manifested as a central low-density region. The use of chain-length bidispersity was then investigated as a way to reduce such packing frustration in the gyroid phase. We found that the longer chains in such systems tend to segregate preferentially inside the gyroid nodes. For a system with components with a 2:1 ratio of chain lengths, we observed an increased range of temperatures where the gyroid phase is stable.

Introduction

Under the appropriate thermodynamic conditions, block copolymers can self-organize at nanoscopic length scales and form microstructures that can lead to numerous materials with useful properties[1] such as mechanical and optical anisotropy, large interface area between different domains, and long-range ordering. In diblock copolymer melts, different microstructures can be obtained by changing the temperature and volume fraction of any one block. The result is a complex phase diagram that presents a variety of well-ordered structures with long-range periodicity. In the simple case of diblock copolymer melts, the following "classical" morphologies[1] can be found: lamellae (L), hexagonally packed cylinders (C), and spheres ordered in a bcc lattice (S). In addition, bicontinuous morphologies with triply periodic spacing have been discovered; e.g., in diblock melts the gyroid[2] (G) phase has been found to be stable. In more complex systems, like star block copolymer melts and block copolymer/nanoparticle nanocomposites, the OBDD[3] (D) and Plumber's Nightmare[4] (P) phases have been respectively obtained. Bicontinuous morphologies are of special interest for the design of novel materials. For example, their interconnectivity in all three directions not only gives them unusual mechanical properties but also makes them perfect candidates as precursors of porous materials,[5,6] catalytic surfaces, and high-conductivity nanocomposites.[7] Theoretical and molecular simulation studies are particularly useful tools to explore the complex phase behavior of both pure diblock copolymers and mixtures of copolymers and other components such as nanoparticles[8−10] and homopolymers.[11] From the numerous computational studies that have been reported, we will briefly review some of the most relevant to this work.

The phase diagram of pure diblock copolymer melts is relatively well understood, both experimentally[12] and theoretically (e.g., the SFCT of Matsen[13,14] and the field-theoretic description of Fredrickson[15]). However, even though the G phase has been proven to be stable in a narrow window of compositions in this kind of theoretical studies,[14,16,17] to the best of our knowledge, it has never been reported in simulations of pure diblock melts. The G phase has only been found in simulations of systems of either triblock copolymers or diblocks with selective solvent, e.g., in the lattice MC simulations of triblock copolymer melts of Dotera et al.,[18] in the lattice MC work with surfactants in selective solvent of Larson et al.,[19] in the MD simulations of Rychkov and Yoshikawa[20] in a selective solvent, and in the lattice Boltzmann simulations of surfactants in mixtures of selective solvents of González-Segredo and Coveney.[21] One should consider, however,[11] that the inclusion of selective solvent or small amounts of homopolymer can stabilize the G phase, widening the range of conditions where such a phase can be observed by simulation. It has also been shown[16,22] that the region of the phase diagram where the G phase is stable for triblock copolymers is significantly wider than that for diblocks, which again facilitates finding the G phase in simulations.

In several simulations of diblock copolymers without selective solvent, no clear indication has been provided on the existence of bicontinuous phases. Such is the case of the Brownian dynamics simulations of Glotzer et al.[23,24] and the dissipative particle dynamics simulations of Groot et al.[25] where only classical morphologies were found. The same is true for the discontinuous molecular dynamic simulations of Schultz et al.[26,27] where they studied diblock copolymer melts and block copolymer/nanoparticle nanocomposites. In this case, the perforated lamellae phase (PL) was found in the region of the phase diagram where the G phase is expected, in disagreement with both theory and experiments.[28]

Block copolymer microphases present long-range order with periodicity that has well-defined characteristic lengths associated with it. The size of the unit cell (i.e., repetitive unit) of these structures is therefore predetermined by the thermodynamic conditions at which the system is set. As a consequence, simulation box lengths need to be a multiple integer of the unit cell size in order to fit the structure and still satisfy the periodic boundary conditions. Simulations have proven[18] that inadequate choices of box dimensions can stabilize meta-

* Corresponding author. E-mail: fe13@cornell.edu.

10.1021/ma051214+ CCC: $30.25
Published on Web 09/02/2005

stable phases. As a result, the size of the simulation box becomes an essential parameter in this kind of system. An attempt to solve this problem was made by Schultz et al.,[29] who developed an algorithm to change the shape of the simulation box while keeping fixed the total volume. Nonetheless, because of their cubic symmetry, bicontinuous morphologies cannot be fitted in a simulation box by changing its relative dimensions if the total volume is kept constant. The latter reason could be a possible explanation for the failure of previous work in obtaining the G phase.

In the present work we use lattice Monte Carlo (MC) simulations together with a simple model for the block copolymer chains to explore the phase diagram of pure diblock melts. Simulations were performed in the weak, intermediate, and strong segregation regime. In addition to the classical morphologies, the G phase was also found in a region of the phase diagram that agrees with experimental results and theoretical predictions. We also explored the use of polydispersity as a way to stabilize the gyroid phase in a wider region of the phase diagram as proposed by Hasegawa et al.[30]

Model and Methods

Model. Space is discretized in a simple cubic lattice where each site can be occupied only by a single bead of the polymer chain. Each bead in the chain represents a Kuhn segment. Bonds are allowed between nearest neighbors that are located at the edges of each site as well as between diagonals sites, yielding to a total of 26 neighbors per lattice site. Details about the applicability of this kind of lattice for block copolymers can be found elsewhere.[31,32]

The total energy of the system is calculated by using pairwise additivity between the bead interactions. Each bead interacts only with its 26 nearest neighbors. The contact energy ϵ_{ij} is defined as

$$\epsilon_{ij} = \begin{cases} 1 & \text{if } i \neq j \\ 0 & \text{if } i = j \end{cases} \tag{1}$$

where i and j represent the type of bead.

To facilitate the mobility of the chains, the systems have a void fraction of $\eta = 0.25$. The beads do not interact with the void (i.e., $\epsilon_{\text{i-void}} = 0$); hence, vacuum acts like a nonselective good solvent. As is customary for lattice simulations, the Flory−Huggins interaction parameter (χ) is obtained from[18] χN = (number of nonbonded neighbors) × (fraction occupied) × ϵ_{AB}/kT = (26 − 2) × (1 − η) × 1 × β, i.e.

$$\chi = 18\beta \tag{2}$$

where $\beta = \epsilon_{AB}/kT$, k is the Boltzmann constant, and T is temperature. Note that this mapping between χ and T is only approximate since small-chain effects are not accounted for. The copolymer composition is defined by

$$f = \frac{\text{no. of beads of one component in chain}}{N} \tag{3}$$

where N is the chain length. Since all beads occupy the same volume, f also defines the volume fraction of the given bead type. For the system of pure diblock copolymers, chains had $N = 20$ unless otherwise indicated. Such a chain length is a compromise between computational efficiency (short chain) and a sufficiently fine discretization of block copolymer composition to map out the phase diagram. Therefore, it is not surprising that chains of comparable lengths have been studied elsewhere.[18,26] As a concrete example, $N = 20$ can be seen to approximately correspond to symmetric chains of poly(isoprene-*b*-ethylene oxide) (PI-*b*-PEO) of a molecular weight of MW ∼ 2.5 × 10^3 g mol^{-1}. For the bidisperse system of diblock copolymers, the shorter component had $N = 20$ while the longer one had either $N = 40$ or $N = 26$.

Simulation Details. The sampling scheme used was the traditional Metropolis Monte Carlo algorithm[33] in the canonical ensemble (NVT), where moves are accepted with probability:

$$P = \min\,[1, \exp(-\beta \Delta E)] \tag{4}$$

The moves implemented were (1) individual "hop" moves,[31] where a single bead is attempted to move with equal probability to any of the sites that conserve the nearest-neighbor condition between chemically bonded monomers; (2) "reptation" moves,[19] where one of the two ends of the chain is moved randomly to one of the nearest-neighbor sites, and the rest of the beads "follow" it by occupying the position of the closest bead chemically bonded in the direction of the move; (3) "switching" moves, whereby the order of the beads in the chain is inverted. This last move has the advantage of never requiring a check of excluded-volume interactions, since the chain occupies the same sites before and after the move is implemented. The "hop", "reptation", and "switching" moves were performed with a relative frequency of 100:10:1, respectively.

Copolymer mesophases and bicontinuous phases in particular are not easy to characterize because of the lack of a convenient order parameter that can provide a clear identification of any such phase. As a consequence, most of the characterization is usually done through simple visual inspection of snapshots of the simulated system. Another powerful tool, widely used by experimentalists in the area of copolymers, to characterize these phases is the structure factor, $S(\mathbf{q})$. The structure factor is calculated straightforwardly from simulations with the equation[34]

$$S(\vec{q}) = \frac{(\sum_j \cos(\vec{q}\cdot\vec{r}_j))^2 + (\sum_j \sin(\vec{q}\cdot\vec{r}_j))^2}{N} \tag{5}$$

where $\vec{q}$ is the wave vector and $\vec{r}_j$ are the positions of the monomers of the minority component in the system. With this definition, $S(\mathbf{q})$ corresponds to the modulus of the Fourier transform of the positions of the minority component beads. Moreover, after calculating $S(\mathbf{q})$, the concentration profile can be reconstructed directly[35] by an inverse Fourier transformation while neglecting wave vectors ($\vec{q}$) with a modulus larger than some cutoff (in this work $q_{\text{cutoff}} = 1.2$). This procedure has the advantage of smoothing out the fluctuations in a particular configuration. All snapshots shown in this work were obtained using this procedure. Another advantage of calculating $S(\mathbf{q})$ is that it provides useful information about the "natural" length of the unit cell of the periodic structures. Such length can be extracted from the location of the first refraction peak, by means of the equation

$$L_{\text{box}} = (2\pi/q^*)m \tag{6}$$

where L_{box} is the estimated length of the unit cell, q^* is the modulus of the wave vector at which the principal $S(\mathbf{q})$ maximum is located, and m is the first observed reflection spacing ratio for a given periodic structure[2] (e.g., $m = 1$ for lamellae, $m = \sqrt{6}$ for the gyroid).

Simulations were equilibrated in the athermal limit and then quenched to the desired temperature where the microstructures are expected to form. It is important to emphasize that, contrary to the case of SCFT calculations, the different morphologies need not be prespecified since the system naturally evolves toward the final state. Typical simulation runs consisted of 10^6 MC moves per bead in the system. Some simulations were run twice as long to ensure stability. At each thermodynamic condition (i.e., a given set of χN and f values), a preliminary simulation was run at a simulation box of a typical size of $30 \times 30 \times 30$ (lattice units)^3 to obtain a hint of the "natural" spacing of the system by means of $S(\mathbf{q})$. Afterward, different unit cell sizes corresponding to different morphologies can be estimated by use of eq 6 (an iteration of this process may be needed). Thus, different simulations (with the same value of χN and f), with different box sizes, consistent with the spacing of different morphologies, were run. However, in most of the cases the system evolved to the same morphology regardless of the simulation box size. Whenever more than one defect-free morphology was found at the same thermodynamic conditions, the stable phase was determined by performing simulations in bigger boxes (i.e., two or more unit cells) and evaluating the chemical potential. Simulation box sizes ranged from $20 \times 20 \times 20$ (lattice units)^3 to $66 \times 66 \times 66$ for larger systems wherein the stability of the system was being tested.

Results

Pure Diblock Melts. To map out the phase diagram of pure diblock copolymer melts simulations were performed in the weak, intermediate, and strong segregation regimes ($\chi N \sim 20-200$). Since for our model the phase diagram is symmetric in volume fraction (f), we ran simulations only for compositions $f \leq 0.5$.

We obtained the classical morphologies of lamellae (L), cylinders (C), and spheres (S) as can be seen in Figure 1 where only the minority component of the block copolymer is shown. Since the L and C phases possess periodicity only in one or two directions, respectively, they can rotate to better accommodate themselves in the simulation box to approach their natural spacing. To test whether this "rotation" was artificially stabilizing any of these structures, different system sizes were tried. However, no "artificial" stabilization was observed. Although some authors[25,36] have suggested that hydrodynamic interactions could be crucial to simulate structures with periodicity in more than one dimension (specifically the C phase), Horsch et al.[24] have recently shown that hydrodynamics was not required to obtain these phases in simulations of diblock copolymers. The lattice MC method employed in this work provides a much more effective configurational sampling than continuum space models and can readily obtain the C phase (despite the absence of hydrodynamics interactions).

In addition to the classical morphologies, in a very small region of the phase diagram the gyroid phase (Figure 2) was found. To ensure that this structure actually corresponds to the G phase, $S(\mathbf{q})$ was calculated (Figure 3) and compared to the experimental results of

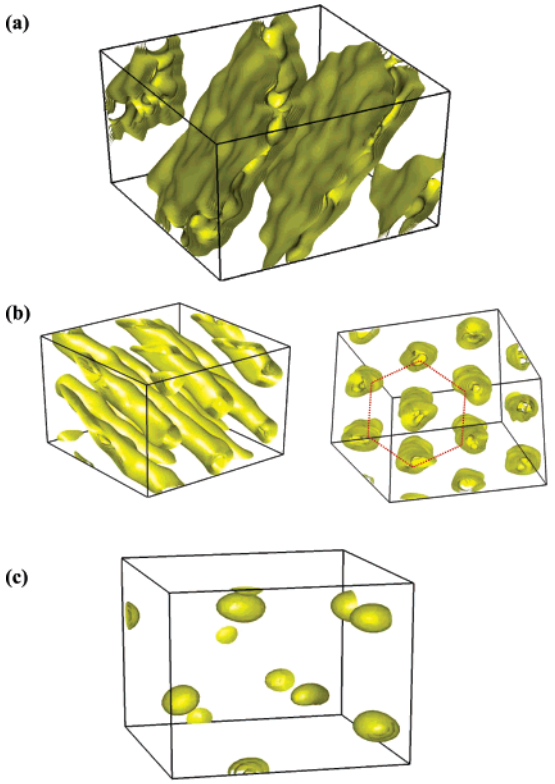

Figure 1. Snapshots of classical morphologies found in the simulations. Only minority component is shown. (a) Lamellae, (b) cylinders, and (c) spheres.

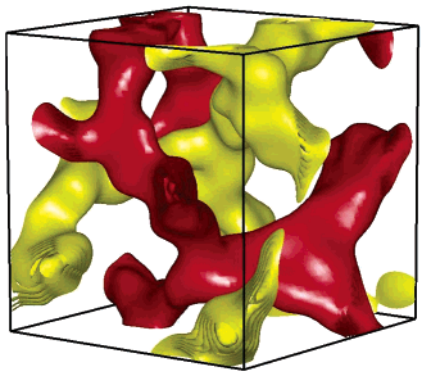

Figure 2. Snapshot of the unit cell of the gyroid phase. Only the minority component is shown. The minority component forms two distinct channels (red and yellow) that never intersect.

Gruner et al.[2] Comparison of the location of the peaks shows good agreement with the ratios that are observed experimentally (i.e., $\sqrt{3}$:$\sqrt{4}$:$\sqrt{10}$:$\sqrt{11}$:$\sqrt{16}$:$\sqrt{19}$). Moreover, when these ratios are reinterpreted as $\sqrt{6}$:$\sqrt{8}$:$\sqrt{20}$:$\sqrt{22}$:$\sqrt{32}$:$\sqrt{38}$ (i.e., multiplied by a factor of $\sqrt{2}$, as suggested by Gruner et al.[2]), it can be seen that the size of the unit cell given by eq 6 (with $q^* = 0.4664$ from Figure 2) coincides exactly with the size of the simulation box (i.e., 33 lattice units per side). In Figure 2, we can also see that the minority component forms a structure composed by "channels" and "nodes", each node is formed by the junction of three channels, as is expected for the gyroid phase.

At the same thermodynamic conditions where we obtained the G phase (i.e., $f = 0.30$, $\chi N = 40$), we also found other structures when simulations were done in boxes of different sizes (e.g., C and perforated lamellae).

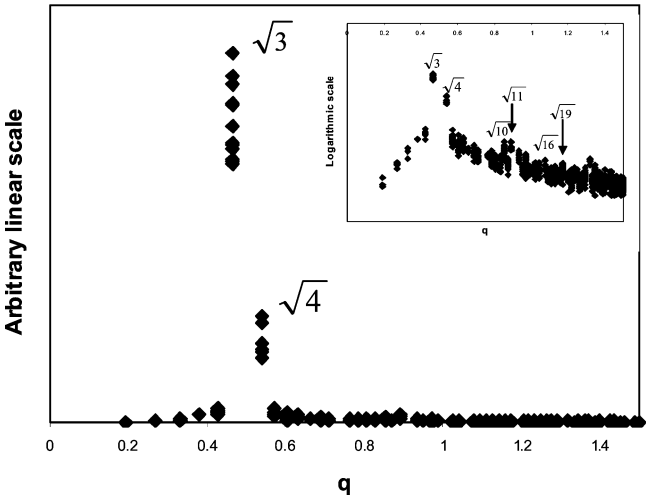

Figure 3. Structure factor calculated from simulated snapshots of the G phase. The inset shows the structure factor in a logarithmic scale. The ratio of the locations of the peaks is in good agreement with the experimental results[2] (i.e., $\sqrt{3}$:$\sqrt{4}$:$\sqrt{10}$:$\sqrt{11}$:$\sqrt{16}$:$\sqrt{19}$).

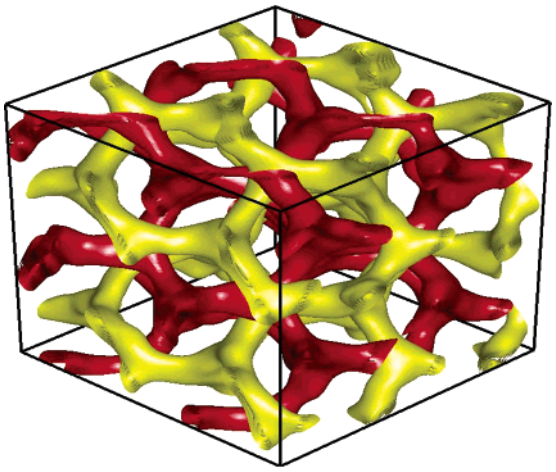

Figure 4. Eight (8) unit cells of the gyroid phase; the box size is 66 × 66 × 66 and contained 10 781 chains. The G phase remained stable in this bigger system. Only the minority component is shown.

However, the PL was only encountered in simulations with boxes much smaller than the G unit cell (fewer than 20 lattice units each side), leading us to conclude that PL is not stable in this thermodynamic state. To test the stability of the G phase respect to the C phase, two bigger boxes (33 × 33 × 66 lattice units) were simulated. In these simulations, instead of quenching from the athermal limit, simulations were started with the respective phases (C or G) already formed. While the C phase did not persist (i.e., cylinders started to connect to each other), the G phase remained stable. In addition, simulations with an even bigger simulation box (66 lattice units per side) were run; again, the gyroid phase remained stable (Figure 4). Simulation of the chemical potential in fully equilibrated systems using Rosenbluth sampling[33] was used to identify the most stable phase, i.e., the one with the lowest free energy. We neglected the PV contribution to the Helmholtz free energy differences since it is expected that for the G and C phases the pressure will be similar and small. It can be seen in Figure 5a that the box dimensions for which the G phase was found (i.e., 33 lattice units per side) correspond to a minimum in chemical potential. Using

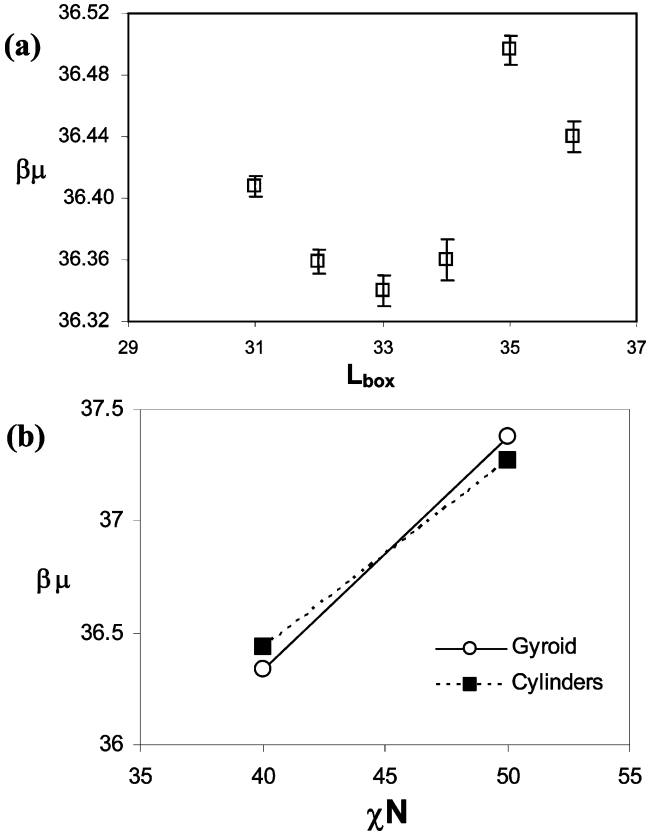

Figure 5. Comparison of the chemical potentials ($\beta\mu$) between the G and C phases for $f = 0.30$. (a) The chemical potential for the observed structure for each box size is presented as a function of the box linear dimension (L_{box}) for $\chi N = 40$. The structures observed at different sizes are interconnected cylinders for $L_{box} = 31$, G phase for $L_{box} = \{32, 33, 34\}$, and C phase for $L_{box} = \{35, 36\}$. (b) Linear interpolation of $\beta\mu$ for the C and G phases between $\chi N = 40$ and $\chi N = 50$; for each phase and a given χN, the $\beta\mu$ value used is the smallest one obtained as a function of system size. The intersection occurs at $\chi N \sim 45$.

the lowest $\beta\mu$ value for which either G or C are stable, we find that $\beta\mu_{gyroid} = 36.34(1)$ and $\beta\mu_{cylinder} = 36.44(1)$, which indicates that the free energy of the G phase is slightly lower than that of the C phase at $f = 0.30$ and $\chi N = 40$. As pointed out before,[18] inadequate choices of simulation box dimensions can stabilize metastable structures due to their inability to fit the unit cell of the stable structure. This effect becomes less important for much larger simulations boxes where two or more unit cells can fit. Since the G phase was the only one that remained stable in the much bigger systems (besides having a slightly lower chemical potential), we conclude that G is the stable phase at the conditions under consideration.

For $f = 0.30$ and $\chi N = 50$, only the C phase formed spontaneously. When quenching the simulated systems for different box sizes, a gyroid-like structure was often initially observed; however, in all cases these unstable intermediates eventually evolved toward the C phase. Further tests were run at $f = 0.30$ and $\chi N = 50$ starting with the L or the G phase already formed (at different χN). In these simulations, only the G phase remained stable during the length of the simulation (10^6 MC steps), but its chemical potential [$[\beta\mu_{gyroid} = 37.38(1)]$ was larger than that of the C phase [$\beta\mu_{cylinder} = 37.27(1)$], confirming that that C phase is the one thermodynamically stable in this point of the phase diagram.

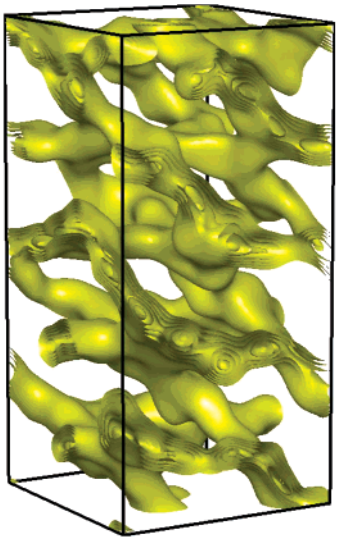

Figure 6. Snapshot of the cocontinuous structure found at $f = 0.35$ and $\chi N = 40$. This structure was found only in a narrow region of the phase diagram between the L and G phases. Only the minority component is shown.

Although we observed the G phase in only one point of the phase diagram (i.e., $f = 0.30$, $\chi N = 40$), we expect that it will be stable in a small finite interval of χN around this point [i.e., $\Delta(\chi N) < 10$]. A rough estimate of the location of the high-χN G−C transition is $\chi N \sim 45$, found by linear interpolation (shown in Figure 5b) of the chemical potential data for $\chi N = 40$ and 50 given before.

For $f = 0.35$ and $\chi N = 40$, neither the G, L, or C phase was fully stabilized; instead, cocontinuous structures were obtained where the minority component forms a single network of channels connected by 3-fold nodes. Recently, Tyler and Morse[37] have shown using SCFT that an orthorhombic *Fddd* phase (O^{70}) should be stable in a very narrow range of f and χN between the G and L phases. Regular cocontinuous structures can be simulated depending on the box shape adopted; Figure 6 shows one such structure obtained for a box with side lengths in the ratio 35:35:70 (and for $f = 0.35$ and $\chi N = 40$). Although the structure in Figure 6 resembles the O^{70} phase, analysis of $S(\mathbf{q})$ shows some discrepancies in the location of the refraction peaks reported experimentally for systems of triblock copolymers by Bates et al.[38] Considering that the O^{70} phase is predicted to be stable in a very narrow region close to the ODT, it is possible that such a phase is suppressed in systems of "short" chains like ours or that it is "skipped" by the coarse discretization of f values afforded by our 20-mer chains. Clearly, a more extensive simulation study is needed to clarify the effect of box size, shape, chain length, and composition on the formation of the O^{70} phase.

When all the resulting structures for the diblock copolymer melt are collected as a function of χN and f, we obtain the approximated phase diagram shown in Figure 7. This diagram is in qualitative agreement with the results of SCFT.[14] However, besides the appearance of the cocontinuous structures previously mentioned, other differences are observed: the ODT is located at higher values of χN ($\chi N \sim 23$), the S phase is also shifted to higher values of χN, and a temperature-driven cylinder−gyroid−cylinder (C−G−C) transition is predicted. The upshifting of the ODT and the S phase is in

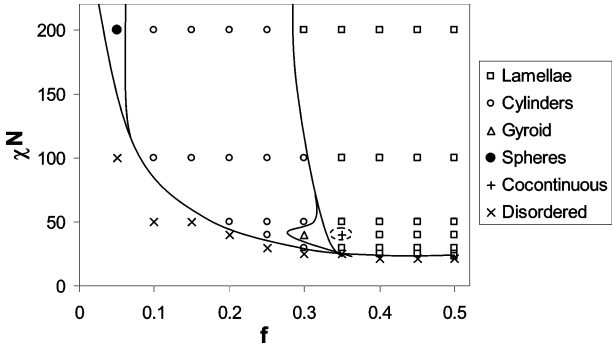

Figure 7. Approximate phase diagram obtained from our simulations. The lines demark rough phase boundaries to guide the eye. The ODT is located at $\chi N \sim 23$. The gyroid phase was found to be stable for $\chi N = 40$ and $f = 0.30$.

agreement with previous simulation results of Hall et al.[26] and Vassilieva and Matsen,[39] where chains of similar size were used. In addition, weak segregation regime theory[17,40] has predicted these two effects for chains of short length wherein fluctuations become important, and therefore mean-field theories become no longer applicable.

Regarding the C−G−C transition, one should note first that SCFT actually predicts its occurrence but only for an extremely narrow range of f values (around $f \sim 0.32$ and $45 < \chi N < 65$). Furthermore, while SCFT clearly predicts a C−G transition at low values of χN, the exact location of the high-χN boundary of the G phase (i.e., the C−L−G high-χN triple point) has not been established by rigorous SCFT calculations but only by extrapolations[14] (in the interval $40 < \chi N < 60$ of the G phase boundaries). It is therefore not unexpected that in such a region of the phase diagram (where free energy differences among the L, G, and C phases are vanishingly small) discrepancies may arise between the predictions of a mean-field theory and the behavior of systems of finite chain length. In addition, the experimental work of Bates et al.,[12] with the metastable PL phase reinterpreted as the G phase,[28,41] suggests that not only C−G transitions at low values of χN can occur but also that G−C transitions at high values of χN are plausible (e.g., for PI-*b*-PS and PEP-*b*-PEE). In fact, most of the experimental work on the G phase has not examined the region where the G phase ceases to be stable at high segregations. In short, the possibility that systems can exhibit a C−G transition at low χN and a G−C transition at higher χN should not be ruled out a priori.

Structure of the Nodes. In the gyroid phase the minority component forms a structure composed of channels and nodes. The thickness of the channels is determined by the length of the minority component blocks. However, since each node is formed by the junction of three channels, nodes need to be bulkier in order to approach the constant mean curvature (CMC) structure[13] that minimizes the interfacial energy.

It has been suggested elsewhere[13,30] that the reason for the very limited stability of the G phase in the phase diagram of pure diblock melts is packing frustration. Since the nodes of the G phase are wider than the channels, chains would need to stretch in the nodes to reach the center. Our simulated G phase allowed us to examine whether this phenomenon occurs inside the nodes. Concentration profiles of the minority component in the simulated nodes show that there is indeed a low-

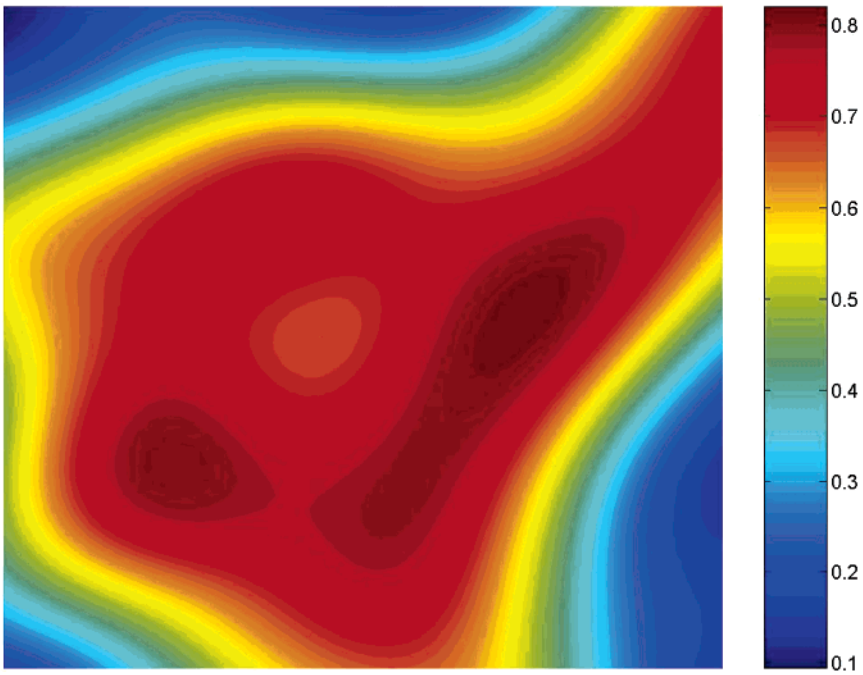

Figure 8. Concentration profile of the minority component in a typical node of the G phase. The concentration in the middle of the node is lower than in its surroundings, indicating the presence of a higher concentration of vacancies. The scale represents the concentration of the minority component, ranging from 0 to 1.

density region (i.e., a higher concentration of vacancies) inside the nodes. This is evident in Figure 8, where a typical concentration profile on a cross section of a node is shown. As can be seen, the concentration in the middle of the node is lower than in its surroundings, evidencing the presence of vacancies. This fact was true for all the nodes present in all the snapshots of the gyroid phase collected from independent runs. The presence of lower concentration regions in the center of the nodes indicates packing frustration of the copolymer chains and therefore a destabilization effect of the G phase. While some degree of vacancy accumulation also occurs at the A−B interfaces of all microsegregated phases because it reduces the number of unfavorable contacts in the system, the vacancy accumulation in the node centers of the G phase is not driven by the same mechanism.

Chain stretching calculations (i.e., via the evaluation of end-to-end distances of the minority blocks) were carried out only for a limited number of statistically independent configurations (10 snapshots). This is because the only reliable way we found to identify of the positions of the gyroid nodes was by visual analysis. The results from these calculations failed to detect chain stretching inside the nodes as it had been speculated, suggesting that, at least in our model, the penalty in entropy of mixing associated with having "vacancies" inside the nodes is less than the penalty in configurational entropy associated with stretching the chains to reach the center of the node. However, the absence of chain stretching inside the gyroid nodes could also be due to the short length of the minority component block (six beads for $f = 0.30$), given that the associated entropic penalty is larger for shorter, non-Gaussian chains. Moreover, since in our model the contact energy between beads of the same type is *zero*, void spaces in the lattice act as a "good" solvent and the intranode interactions are basically entropic. Hence, it is also possible that a model with more dominant energetic interactions (i.e., negative contact energies between equal-type beads and thus void spaces acting as "poor" solvent) could lead to a different nodal structure with less vacancies and more chain stretching. In either case, however, packing frustration inside the gyroid nodes should still be prevalent.

Bidisperse Mixtures of a Diblock Copolymer Melt. Several strategies have been proposed to reduce packing frustration inside the G phase nodes, including the use of nanoparticles or low molecular weight homopolymers that could reside preferentially in the nodes of the gyroid. In addition, Hasegawa et al.[30] suggested that copolymers having a bidisperse distribution of chain lengths could have a more stable G phase. In this case, the hypothesis is that longer chains can segregate to the nodes to fill the vacancies (Figure 9) while the shorter chains concentrate in the channels to avoid packing frustration in the nodes, therefore stabilizing the gyroid phase. To our knowledge, this hypothesis has not been tested in simulations. Experimentally, Ponsinet et al.[42] have study the effect of polydispersity in diblock copolymers, finding the L and C phases (and coexistence L + C in between) but not the G phase; note that these authors focused in the strong segregation regime where the G phase is expected to be unstable. Also, Sides and Fredrickson[43] studied the effect of polydispersity using SCFT but only focused on the classical morphologies (L, C, and S).

We studied two model systems with the purpose of testing this hypothesis (Figure 10). The first one (system 1) was composed of 90% chains of length $N = 20$ and 10% chains with $N = 40$, with a volume fraction of minority component $f = 0.30$ (the same f where the G phase was found). The second system (system 2) had also 90% of chains of length $N = 20$ and $f = 0.30$, but it contained 10% of chains with $N = 26$ and $f = 0.4615$ (12 beads of minority component). System 2 was studied to test whether just making longer the block of the minority component was enough to reduce packing

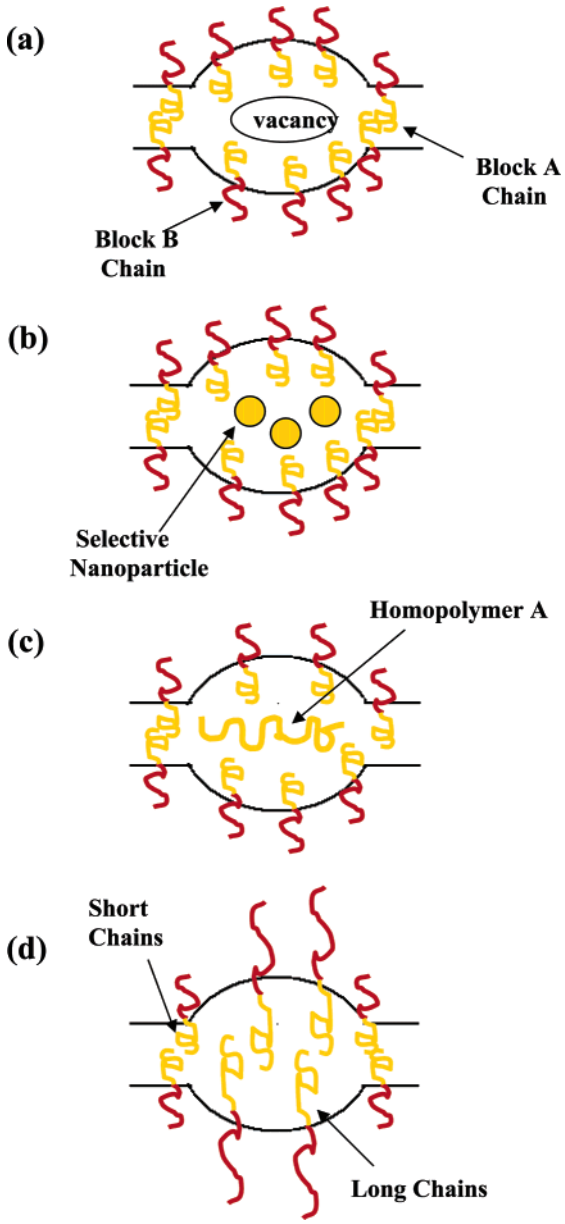

Figure 9. Cartoon representing how filling the "vacancies" in the nodes can stabilize the gyroid phase. (a) Chains stretching in the gyroid nodes to fill the vacancies. (b) Selective nanoparticles filling the vacancies. (c) Homopolymer filling vacancies. (d) Bidisperse distribution of chain length where the longer chains concentrate in the nodes. Based on a figure shown by Hasegawa et al.[30]

frustration (note that for system 2 the overall composition is $f = 0.3162$). Simulations were performed around the same temperature where G was found ($\beta = 0.111\,11$, $\chi N \sim 40$). No attempt was made to "optimize" the bidisperse systems compositions.

After equilibration, the G phase was also found in both systems with a unit cell size of 35 lattice units (in the pure melt the unit cell was 33 lattice units). In each system, the appropriate simulation box dimensions were estimated using $S(\mathbf{q})$ together with eq 6, as explained in the section on simulation details. To see whether there was actually segregation between longer and shorter chains, we calculated the intermolecular bead-to-bead radial distribution function for the minority component. As can be seen in Figure 11, in both systems the longer chains aggregate more than the shorter

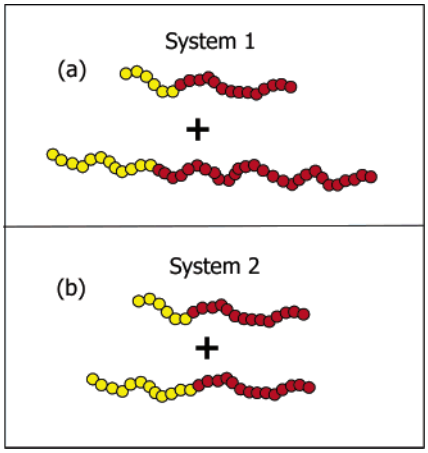

Figure 10. Cartoon representing the two model systems studied with a bidisperse distribution of components. (a) System 1: 90% chains with $N = 20$ and 10% chains with $N = 40$; the volume fraction of minority block in both components is $f = 0.30$. (b) System 2: 90% of the original $f = 0.3$ chains with $N = 20$, mixed with $f = 0.46$ chains ($N = 26$). Thus, in system 2 the overall minority component fraction is $f_{all} = 0.316$.

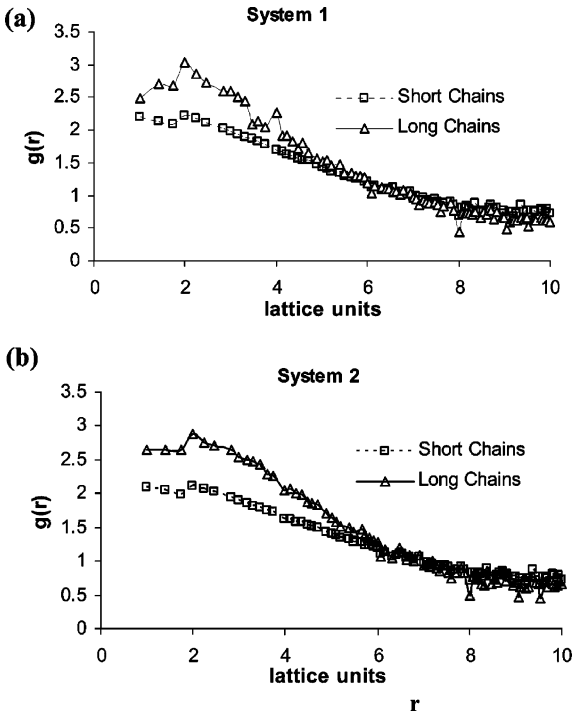

Figure 11. Intermolecular bead-to-bead radial distribution functions for the minority component: (a) system 1 [$g(r)_{max} = 3.04$]; (b) system 2 [$g(r)_{max} = 2.89$]. The stronger short-range correlation in the longer chains indicates some degree of clustering (aggregation) beyond what is observed in the shorter chains.

chains. This is evident in the stronger short-range correlations (i.e., higher peak) observed in the radial distribution function of the longer chains. We also examined the hypothesis that this aggregation leads to a spatially correlated segregation wherein the minority component blocks of the longer chains reside preferentially inside the gyroid nodes. Figure 12 shows a typical snapshot of the system where only the minority component blocks are shown; the longer chains are "painted" in red and the shorter chains in yellow. As can be seen in Figure 12, most of the longer chains are indeed found inside the nodes, thus corroborating the hypothesis. This

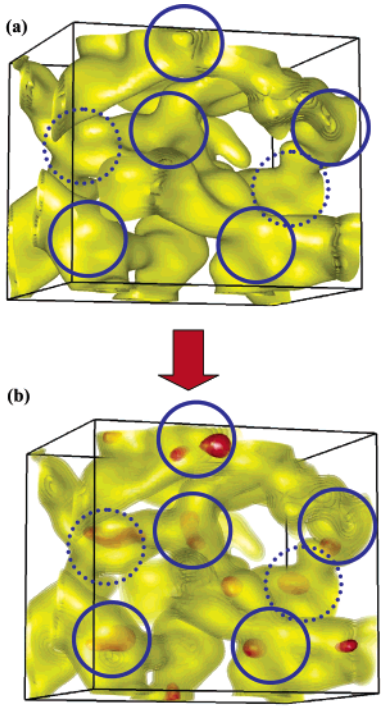

Figure 12. Snapshot of the gyroid phase before (a) and after (b) "painting" in red the longer chains and making the structure semitransparent. Shorter chains are kept in yellow, and only the minority component is shown. Longer chains tend to reside in the nodes.

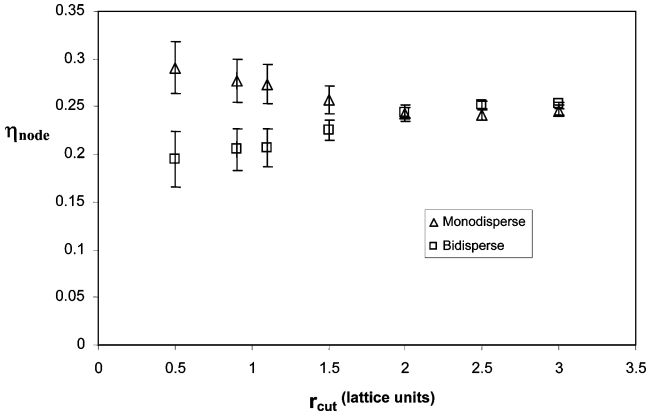

Figure 13. Mean void fraction η_{node} inside the gyroid nodes as a function of the radius (r_{cut}) of the spherical region around the node center. Values of η_{node} are the average void fraction over all the volume inside such a spherical region and for all the nodes in selected configurations of a given system.

was true for both systems studied (results for other snapshots lead to similar conclusions).

To investigate how bidispersity affects packing in the gyroid nodes, selected typical configurations were used to obtain concentration profiles of "voids" (smoothed out as described in the section on simulation details). To estimate the mean void fraction inside the nodes, η_{node}, averages were obtained inside regions of space delimited by spheres of radius r_{cut} centered at the innermost point in the nodes. It is expected that the value of η_{node} will strongly depend on the choice of r_{cut}; a larger r_{cut} will give a η_{node} consistent with the *global* void fraction ($\eta = 0.25$) while a smaller r_{cut} will give a η_{node} representative of the *local* void fraction at the node center. In Figure 13, η_{node} values for the monodisperse system and the bidisperse system 1 are plotted as a function of r_{cut}.

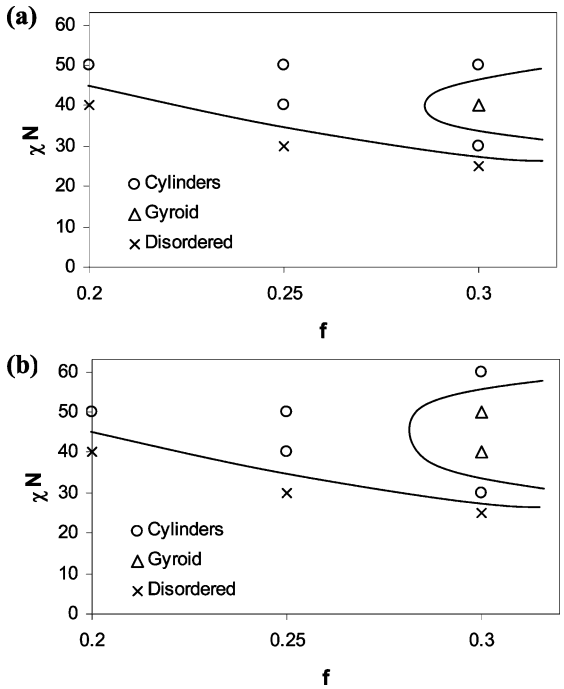

Figure 14. Effect of bidisperse distribution of chain lengths on gyroid stability. (a) Zoom-in of phase diagram for the pure melt in region of gyroid stability. (b) Modified phase diagram for the bidisperse mixture (system 1); the region of stability of G increases to lower temperature. The lines (rough phase boundaries) are only guides to the eye. The χN scale in (b) is also based on $N = 20$. An imperfect C structure was obtained for the point corresponding to $f = 0.3$ and $\chi N = 60$.

As can be seen, η_{node} values for small r_{cut} (i.e., highly localized at the center) for the bidisperse system are consistently smaller than those for the monodisperse system; this suggests that packing frustration in the former has been reduced relative to that in the latter (where vacancies concentrate in the node center). However, the results shown in Figure 13 should only be taken as qualitatively trends, given the significant density fluctuations in the gyroid nodes and the difficulty of unambiguously defining node centers. A different, indirect quantification of the effect of bidispersity on packing frustration is discussed next.

If the segregation of the longer chains to the nodes is indeed stabilizing the gyroid phase, then the latter could in principle be stable in a wider region of the phase diagram. To test this idea, we ran simulations of both model systems at temperatures where cylinders were stable; i.e., at temperatures immediately above ($\chi N \sim 30$) and below ($\chi N \sim 50$) the region where the G phase was initially found (see Figure 5). At the higher temperature (lower χN), we found that again the cylinder phase (not G) was stable; i.e., we did not detect widening of the G phase window in the region of higher temperatures. On the other hand, when we explored regions of lower temperature we found that while in system 2 the cylinders were still stable, in system 1 the gyroid was stable (Figure 14). Hence, we found that in system 1 the G phase became stable in a wider region of temperatures in the phase diagram, consistent with the idea that segregation of longer chains to the nodes reduces packing frustrations and therefore stabilizes the structure. This is a significant effect, considering that only a very small amount of longer chains was added. (A volume fraction of 10% actually corresponds to a mole fraction of about 5% of longer chains.) It is unclear at

this point why system 1 provides better stabilization of the G phase than system 2, while both systems exhibit comparable extents of long-chain nodal segregation; it is possible that a longer majority block (in the long chains of system 1) may also provide added stability to the structure surrounding the node. In both systems, however, we did not find stabilization of the G phase in composition space, since we did not obtain this structure when we ran simulations at volume fractions $f = 0.25$ and $f = 0.35$ (i.e., compositions adjacent to the f where the G phase was found for the monodisperse system).

Conclusions

We have mapped out the phase diagram of pure diblock melts using canonical Monte Carlo simulations of a coarse-grained lattice model of the block copolymer chains. As expected, we found that the diblocks assembled into the classical morphologies of lamellae, cylinder, and spheres depending on the values of block composition (f) and χN. In a small region of the intermediate segregation regime (i.e., at $\chi N \sim 40$ and $f \sim 0.30$) the bicontinuous gyroid phase was found to be thermodynamically stable. Also, a cocontinuous structure that bears some resemblance to the O^{70} phase was encountered between the L and G phase (i.e., at $\chi N \sim 40$ and $f \sim 0.35$). To the best of our knowledge, this work constitutes the first time the gyroid phase has been simulated for systems of pure diblock melts; the range of compositions and temperatures in which this phase is stable was found to be very narrow. The periodicity of the G phase in the three directions makes it especially sensitive to the choice of simulation box size. As a consequence, other phases like cylinders and perforated lamellae were also found at the same thermodynamic conditions when the simulation box was not of the right size to fit an integer number of gyroid unit cells. However, such alternative phases were shown to be metastable, since they presented higher values of chemical potential and did not remain stable in larger simulation boxes. Concentration profiles of the minority component blocks revealed the presence of low concentration regions and the absence of chain stretching inside the gyroid nodes. The low-concentration regions cause an entropic packing frustration, henceforth limiting the stability of the G phase in the phase diagram.

We also studied mixtures of block copolymers with chain length bidispersity to test the hypothesis that this kind of systems can stabilizes the gyroid phase (as suggested by Hasegawa et al.[30]). The intermolecular bead-to-bead radial distribution function showed that longer chains tend to aggregate more than the shorter chains. Moreover, analysis of configurations of the system revealed that the longer chains reside preferentially in the nodes of the gyroid and fill up better the node centers (i.e., a reduction of packing frustration). Finally, we found that for one of the systems studied with chain length bidispersity (system 1), the gyroid phase is indeed stable in a wider range of temperatures than in the pure diblock melt. This result supports the idea that chain length bidispersity can be used as an effective means to stabilize the G phase. In principle, optimal bidisperse compositions could be found to maximize such an effect.

Several well-known limitations are associated with the simplified lattice model adopted here, e.g., the highly coarse-grained nature of the packing and energetic interactions. Furthermore, it should be noted that experiments are usually performed at constant pressure (P), while simulations in this work were performed at constant density (ρ) because of the difficulties associated with performing constant P simulations in lattice systems. Although most theories and simulations are also carried out at constant ρ, we expect[44] that for chains of finite size the two different phase diagrams (constant ρ and constant P) can become significantly different. Simulations of block copolymers in the continuum space could be used to determine the importance of this effect.

Acknowledgment. This work was partially supported by the ACS Petroleum Research Fund. Additional support from the US Department of Energy, Grant DE-FG02-05ER15682, is gratefully acknowledged. The authors are also grateful to Prof. U. Wiesner (MSE, Cornell University) for several stimulating discussions.

References and Notes

(1) Hamley, I. W. The Physics of Block Copolymers; Oxford University Press, 1998.
(2) Hajduk, D. A.; Harper, P. E.; Gruner, S. M.; Honeker, C. C.; Kim, G.; Thomas, E. L.; Fetters, L. J. *Macromolecules* **1994**, *27*, 4063.
(3) Thomas, E. L.; Alward, D. B.; Kinning, D. J.; Martin, D. C.; Handlin, D. L., Jr.; Fetters, L. J. *Macromolecules* **1986**, *19*, 2197.
(4) Finnefrock, A. C.; Ulrich, R.; Toombes, G. E. S.; Gruner, S. M.; Wiesner, U. *J. Am. Chem. Soc.* **2003**, *125*, 13084.
(5) Templin, M.; Franck, A.; Du Chesne, A.; Leist, H.; Zhang, Y.; Ulrich, R.; Schadler, V.; Wiesner, U. *Science* **1997**, *278*, 1795.
(6) Kamperman, M.; Garcia, C. B. W.; Du, P.; Ow, H.; Wiesner, U. *J. Am. Chem. Soc.* **2004**, *126*, 14708.
(7) Cho, B.-K.; Jain, A.; Gruner, S. M.; Wiesner, U. *Science* **2004**, *305*, 1598.
(8) Thompson, R.; Ginzburg, V.; Matsen, M.; Balazs, N. *Science* **2001**, *292*, 2469.
(9) Lin, Y.; Böker, A.; He, J.; Sill, K.; Xiang, H.; Abetz, C.; Li, X.; Wang, J.; Emrick, T.; Long, S.; Wang, Q.; Balazs, A.; Russel, T. *Nature (London)* **2005**, *434*, 55.
(10) Wang, Q.; Nealey, P. F.; de Pablo, J. J. *J. Chem. Phys.* **2003**, *118*, 11278.
(11) Matsen, M. W. *Macromolecules* **1995**, *28*, 5765.
(12) Bates, F.; Schulz, M.; Khandpur, A.; Forster, S.; Rosedale, J. *Faraday Discuss.* **1994**, *98*, 7.
(13) Matsen, M. W.; Bates, S. F. *Macromolecule*s **1996**, *29*, 7641.
(14) Matsen, M. W.; Bates, F. S. *J. Chem. Phys.* **1997**, *106*, 2436.
(15) Fredrickson, G. H.; Ganesan, V.; Drolet, F. *Macromolecules* **2002**, *35*, 16.
(16) Matsushita, Y. *J. Polym. Sci., Part B* **2000**, *38*, 1645.
(17) Hamley, I. W.; Podneks, V. E. *Macromolecules* **1997**, *30*, 3701.
(18) Dotera, T. *Phys. Rev. Lett.* **2002**, *89*, 205502.
(19) Larson, R. G. *J. Phys. II* **1996**, *6*, 1441.
(20) Rychkov, I.; Yoshikawa, K. *Macromol. Theory Simul.* **2004**, *13*, 257.
(21) González-Segredo, N.; Coveney, P. V. *Europhys. Lett.* **2004**, *65*, 795.
(22) Matsen, M. W. *J. Chem. Phys.* **1998**, *108*, 785.
(23) Starr, F. C.; Schrøder, T. B.; Glotzer, S. C. *Phys. Rev. E* **2001**, *64*, 021802.
(24) Horsch, M. A.; Zhang, Z.; Iacovella, C. R.; Glotzer, S. C. *J. Chem. Phys.* **2004**, *121*, 11455.
(25) Groot, R. D.; Madden, T. J.; Tildesley, D. J. *J. Chem. Phys.* **1999**, *110*, 9739.
(26) Schultz, A. J.; Hall, C. K.; Genzer, J. *J. Chem. Phys.* **2002**, *117*, 10329.
(27) Schultz, A. J.; Hall, C. K.; Genzer, J. *Macromolecules* **2005**, *38*, 3007.
(28) Hajduk, D. A.; Takenouchi, H.; Hillmyer, M. A.; Bates, F. S.; Vigild, M. E.; Almdal, K. *Macromolecules* **1997**, *30*, 3788.
(29) Schultz, A. J.; Hall, C. K.; Genzer, J. *J. Chem. Phys.* **2004**, *120*, 2049.
(30) Hasegawa, H.; Hashimoto, T.; Hyde, S. T. *Polymer* **1996**, *37*, 3825.
(31) Dotera, T.; Hatano, A. *J. Chem. Phys.* **1996**, *105*, 8413.
(32) Larson, R. G. *Macromolecules* **1994**, *27*, 4198.

(33) Frenkel, D.; Smit, B. *Understanding Molecular Simulation*; Academic Press: San Diego, CA, 1996.
(34) McGreevy, R. L. In *Computer Modeling in Inorganic Crystallography*; Academic Press: San Diego, CA, 1997.
(35) Shultz, A. Modeling and Computer Simulation of Block Copolymer/Nanoparticle Nanocomposites. Ph.D. Thesis, Chapter 5, North Carolina State University, Raleigh, NC, 2003.
(36) Groot, R. D.; Madden, T. J. *J. Chem. Phys.* **1998**, *108*, 8713.
(37) Tyler, C. A.; Morse, D. C. *Phys. Rev. Lett.* **2005**, *94*, 208302.
(38) Epps, T. H., III; Cochran, E. W.; Hardy, C. M.; Bailey, T. S.; Waletzko, R. S.; Bates, F. S. *Macromolecules* **2004**, *37*, 7085.
(39) Vasilliev, O. N.; Matsen, M. W. *J. Chem. Phys.* **2003**,*118*, 7700.
(40) Fredrickson, G. H.; Helfand, E. *J. Chem. Phys.* **1987**, *87*, 697.
(41) Matsen, M. W. *J. Phys.*: *Condens. Matter* **2002**, *14*, R21.
(42) Bendejacq, D.; Ponsinet, V.; Joanicot, M.; Loo, Y.; Register, A. *Macromolecules* **2002**, *35*, 6645.
(43) Sides, S. W.; Fredrickson, G. H. *J. Chem. Phys.* **2004**, *121*, 4974.
(44) Escobedo, F.; de Pablo, J. *Macromolecules* **1999**, *32*, 900.

MA051214+